



The effect of gyrolite structure properties on Zn^{2+} ion adsorption

Aliona Iljina*, Kestutis Baltakys, Anatolijus Eisinas

Department of Silicate Technology, Kaunas University of Technology Radvilenu str. 19, LT-50270 Kaunas, Lithuania, Tel. +370 67753520; Fax: +370 7300152; email: aliona.iljina3@gmail.com (A. Iljina), Tel. +370 68789856; email: kestutis.baltakys@ktu.lt (K. Baltakys), Tel. +370 68916035; email: anatolijus.eisinas@ktu.lt (A. Eisinas)

Received 18 December 2013; Accepted 11 October 2014

ABSTRACT

The effect of gyrolite structure properties on Zn^{2+} ion adsorption in an alkaline solution was determined. Gyrolite was synthesized for 32, 48, 72, 120, and 168 h at 200 °C from a stoichiometric composition (molar ratio of C/S = 0.66) of the initial CaO and $SiO_2 \cdot nH_2O$ mixtures. It was established that gyrolite does not regroup into related compounds, when the hydrothermal synthesis duration was varied from 32 to 168 h, although its structure changed as the duration of the synthesis was prolonged. Also, the adsorption capacity of gyrolite for Zn^{2+} ions depends on the structural properties of the adsorbent. By prolonging the duration of synthesis from 32 h to 168 h, the adsorption capacity of gyrolite decreased from 99% (29.92 mg Zn^{2+} /g) to 93% (27.91 mg Zn^{2+} /g). It was found that the adsorption reactions are not reversible processes, and follow by a pseudo-second-order model. X-ray diffraction analysis showed that the crystal structure of gyrolite remained stable after the adsorption processes.

Keywords: Gyrolite; Adsorption; Calcium silicate hydrate; Heavy metals; Kinetics

1. Introduction

Contamination by heavy metals (HM) is becoming an increasingly common environmental problem [1–8]. Heavy metal pollution is covert, persistent, and irreversible. This kind of pollution not only degrades the quality of the atmosphere, water bodies, and food crops, but it also threatens the health and well-being of animals and human beings along the food chain [9,10].

High levels of zinc can be found in certain soils as naturally or as a result of a long-term anthropogenic activity that leads to its accumulation, i.e. such as the use of fertilizers or industrial waste [11–13]. It belongs to the second class of toxicity, characterized by low

mutagenic and carcinogenic properties [14]. By ingesting food and drinking water that have a high concentration of zinc, human health can be endangered: corneal ulcers can form and the esophagus can be damaged by this heavy metal [15].

Various methods have been proposed for the removal of toxic HM from wastewaters: chemical precipitation, coagulation–flocculation, membrane filtration, chelation, biosorption, solvent extraction, electrochemical treatment, ion exchange, and adsorption [16–18]. However, many of these techniques are expensive and are not environmentally friendly. Among the various methods, adsorption is now recognized as one of the most effective and attractive techniques for the removal of HM from the environment [19,20].

*Corresponding author.

Many authors [21–24] have reported that calcium silicate hydrates (C-S-H) prepared under hydrothermal treatment act as cation exchangers with some metal cations (Ca^{2+} or Si^{4+}) in their lattice structure. These compounds became a new family of inorganic cation exchangers.

The mineral, gyrolite, is one of these C-S-H with the most likely chemical formula $\text{Ca}_{16}\text{Si}_{24}\text{O}_{60}(\text{OH})_8 \cdot (14+x)\text{H}_2\text{O}$ [25–27]. This compound is commonly found in volcanic and basaltic rocks, in voids or gaps, and it exists only with related minerals. Gyrolite group compounds at the laboratory scale can be synthesized by the hydrothermal treatment of CaO and SiO_2 mixtures [28].

It was found that gyrolite is stable at 120–200°C under saturated steam pressure. At a lower temperature, a variable (undefined) composition of the semi-crystalline compound-CSH(I) was obtained [29,30]. At temperatures higher than 200°C, truscottite forms, although a metastable gyrolite may be obtained up to 270°C. However, there are little data in the literature on structural changes of gyrolite under conditions of hydrothermal synthesis.

It is known that gyrolite can adsorb more chemical elements than other C-S-H, because the interlayer sheets with a thickness of about 2.2 nm (one of the largest in all of the calcium silicate hydrates) in gyrolite are available for the intercalation of a new guest by controlling the charge of the host [29].

In previous work, [31] it was determined that gyrolite shows very good adsorption properties, as almost all of the Cu^{2+} ions (99.5% removal efficiency) are intercalated, depending on the initial concentration of copper ions in the alkaline medium. However, the experimental data of V. Kasperavičiute showed that in an acidic medium gyrolite acted as a chemisorbent that could adsorb only 41.48% of Cu^{2+} ions [32].

It is important to ascertain the effect of kinetic parameters (k and q_e , where k is the rate constant of adsorption and q_e is the amount of adsorbed ions at equilibrium) on adsorption reactions, because an examination of system kinetics can reveal the adsorption mechanism [21,33]. The kinetic models that are usually examined are the pseudo-first-order and pseudo-second-order models [33–35].

The aim of this work was to examine the effect of isothermal curing duration at 200°C on gyrolite structure properties. Zinc ion adsorption reactions using different crystallinity gyrolite samples are presented.

2. Materials and methods

2.1. Materials and manufacture of synthetic gyrolite

In this work, the following reagents were used as starting materials: fine-grained $\text{SiO}_2 \cdot n\text{H}_2\text{O}$ (ignition losses 21.28%; specific surface area $S_a = 1,307 \text{ m}^2/\text{kg}$ by the Blaine method) and calcium oxide (CaO was burned at 950°C for 0.5 h; $S_a = 1,171 \text{ m}^2/\text{kg}$; purity—97.68%).

The synthesis of gyrolite was carried out in unstirred suspensions in vessels of stainless steel. Pure gyrolite was synthesized during 32, 48, 72, 120, and 168 h at 200°C from a stoichiometric composition (the molar ratio of CaO/SiO_2 was equal to 0.66, where the water–solid ratio of the suspension was equal to 10) of the initial CaO and $\text{SiO}_2 \cdot n\text{H}_2\text{O}$ mixtures. These synthesis conditions were chosen according to previously published data [36]. The products of the synthesis were filtered, rinsed with ethyl alcohol to prevent carbonization of materials, dried at $50 \pm 5^\circ\text{C}$, and sieved through a sieve with a mesh width of 50 μm . The chemical composition of synthetic gyrolites is presented in Table 1.

2.2. Adsorption experiments and kinetics models

Adsorption experiments were carried out at 25°C in the thermostatic adsorber Grant SUB14 for different time periods (0.5, 1, 2, 3, 5, 10, 15, 30, and 45 min). An amount of 1 g of gyrolite was added to 100 ml of $\text{Zn}(\text{NO}_3)_2$ aqueous solution containing 0.3 g/l of Zn^{2+} ions. In order to maintain the alkalinity of the solution (pH 9) and to prevent $\text{Zn}(\text{OH})_2$ precipitation, an aqueous solution ($c = 10\%$) of NH_4OH was used. The percentage of adsorbed ions was determined on the basis of the variations in the concentration of the cations both in the solution and in the gyrolite. The saturated adsorbent was rinsed with distilled water, dried at $50 \pm 5^\circ\text{C}$, and dissolved in HCl (1:1).

In order to determine kinetics parameters of adsorption reactions, few kinetics models have been developed, and fitted for the adsorption process of Zn^{2+} ions into gyrolite. The Lagergren model [33–35] assumes *first-order-adsorption kinetics* and can be represented by the equation:

$$\frac{dq_t}{dt} = k_1 - (q_e - q_t) \quad (1)$$

where q_e and q_t are the amount of adsorbed ions at equilibrium and at time t_e , respectively (mg g^{-1}), and k_1 is the rate constant of pseudo-first-order adsorption (min^{-1}). After integration and applying boundary

Table 1
The chemical composition of synthetic gyrolites

Chemical composition of synthetic gyrolite, %	Duration of synthesis, h				
	32	48	72	120	168
CaO	36.01	36.20	36.34	36.61	36.73
SiO ₂	58.47	58.78	59.01	59.45	59.64
H ₂ O	5.84	5.28	4.87	4.1	3.76

conditions $t = 0$ to $t = t_e$ and $q_t = 0$ to $q_t = q_e$, the integrated form becomes:

$$\log(q_e - q_t) = q_e - \frac{k_1}{2.303} t \quad (2)$$

The *pseudo-second-order adsorption kinetic rate equation* [26–28] is expressed as:

$$\frac{dq_t}{dt} = k_2(q_e - q_t)^2 \quad (3)$$

where k_2 is the rate constant of the pseudo-second-order adsorption ($\text{g mg}^{-1} \text{min}^{-1}$). For the boundary conditions $t = 0$ to $t = t_e$ and $q_t = 0$ to $q_t = q_e$, the integrated form of the equation becomes (the integrated rate law for the pseudo-second-order reaction).

$$\frac{1}{q_e - q_t} = \frac{1}{q_e} + k_2 t \quad (4)$$

2.3. Analytical techniques

The X-ray powder diffraction (XRD) data were collected with a DRON-6 X-ray diffractometer with Bragg–Brentano geometry using Cu K α radiation and a graphite monochromator, operating with a voltage of 30 kV and an emission current of 20 mA. The step-scan covered the angular range of 2–60° (2θ) in steps of $2\theta = 0.02^\circ$. A computer program X-fit was used for the diffraction profile refinement under the pseudo-Void function, and for the description of the diffraction background under the third-degree Tchebyshev polynomial.

The concentration of Ca²⁺ and Zn²⁺ ions was determined using a Perkin–Elmer Analyst 400 atomic absorption spectrometer with the following parameters: Zn²⁺ wavelength = 213.86 nm; Ca²⁺ wavelength = 422.67 nm; hollow cathode lamp current (I) = 30 mA; type of flame was C₂H₂–air; oxidant

air = 10 l/min; acetylene = 2.5 l/min. The pH value was taken by a Hanna instrument (Hi 9321, microprocessor pH meter).

Simultaneous thermal analysis (STA; differential scanning calorimetry (DSC), and thermogravimetry) was also employed to measure the thermal stability and phase transformation of samples at a heating rate of 15°C/min; the temperature ranged from 30°C up to 1,000°C under air atmosphere. The test was carried out on a Netzsch instrument STA 409 PC Luxx. Ceramic sample handlers and crucibles of Pt–Rh were also used.

Scanning electron microscopy (SEM) (Evo 50) coupled with energy dispersive X-ray spectrometry (EDS) was performed using an accelerating voltage of 20 kV and a working distance of 10 mm for SEM observation, and a 200 s accumulation time for EDS analysis.

3. Results and discussion

3.1. Gyrolite hydrothermal synthesis

It was determined that in the CaO and SiO₂·*n*H₂O mixture with 32 h of isothermal curing the intermediate compounds (C-S-H(I), Z-phase) recrystallize to the main synthesis product, gyrolite, the stoichiometric composition of which corresponds to the molar ratio of the initial mixture (C/S ~0.66). In the X-ray diffraction pattern, the diffraction maximums most characteristic to the latter compound (*d*-spacing: 2.273, 1.126, 0.844, 0.420, 0.365, 0.280, and 0.224 nm) are clearly seen, and no other peaks are identified (Fig. 1, curve 1). The crystallinity of gyrolite increases by prolonging the isothermal curing duration from 32 to 168 h, and then the intensities of diffraction peaks significantly increase (Fig. 1, curve 2–5).

The crystallite size (D_{hkl}) of synthesized gyrolite was calculated from the line broadening using Scherrer's equation [37]:

$$D_{hkl} = \frac{k \cdot \lambda}{B_{hkl} \cdot \cos \theta} \quad (5)$$

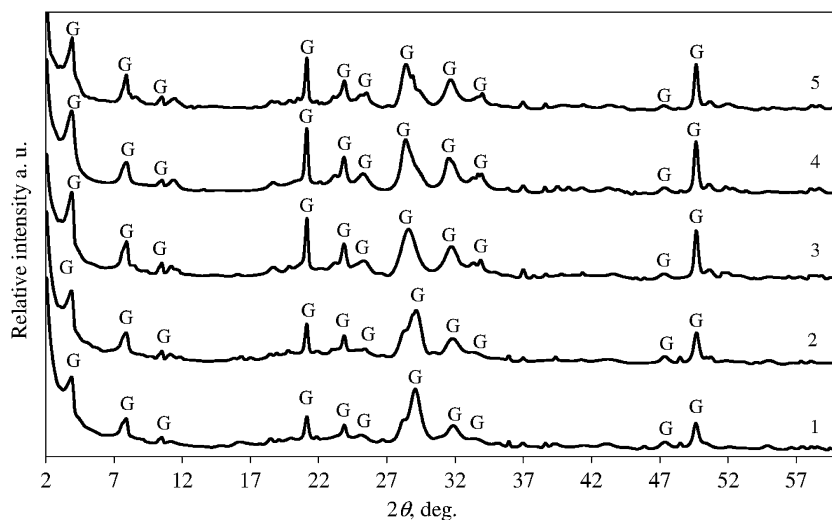


Fig. 1. X-ray diffraction patterns of gyrolite with varying duration of hydrothermal synthesis at 200°C, in h: 1–32, 2–48, 3–72, 4–120, 5–168. Index: G—gyrolite.

where λ is the wavelength of the Cu K α radiation (0.154056 nm), θ is the Bragg's diffraction angle, B_{hkl} is the full width at half maximum intensity of the gyrolite (001) reflection peak $2\theta \sim 3.95^\circ$, and k is a constant (the value used in this study was 0.94).

It was found that by prolonging the synthesis time up to 168 h the crystallite size and diffraction peak area (001) of gyrolite increase to 95 nm and 39 a.u., respectively (Fig. 2(a) and (b)).

The STA analysis data showed that the increase in synthesis duration also affected the thermal properties of gyrolite. It was observed that after 32–120 h of synthesis the heat of endothermic effects at 80–200°C (which reflect the loss of physisorbed and interlayer water from the crystal structure of gyrolite) increased from 48.68 to 71.09 J/g (Fig. 3(a); Table 2). Also, the typical temperatures of this effect shift to higher temperatures: T_{onset} from 108°C to 111°C, T_{peak} from 138°C to 143°C, and T_{end} from 176°C to 175°C. At the same time, the weight loss of this compound shrinks from 5.54 to 3.90 wt% (Table 2).

Thus, after sufficiently long synthesis duration the structural elements of the gyrolite lattice were connected to a more orderly structure of the interlayer X, because consumption of destruction energy increased about 1.5 times (from 48.68 to 71.09 J/g) (Fig. 3(a); Table 2). By prolonging the duration of synthesis for one week, the structure of the gyrolite crystalline lattice remained stable: the heat of the endothermic effect (from 71.09 to 69.34 J/g) and the weight loss (from 3.90 to 3.56 wt%) were slightly decreased.

It was estimated that the heat of exothermic effects at 830°C–890°C (which are associated with recrystallization

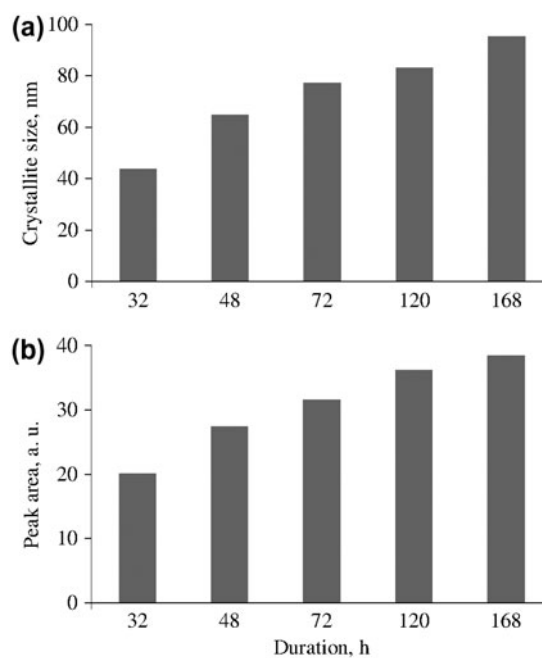


Fig. 2. Dependence of crystallite size (a) and diffraction peak area (001) (b) of gyrolite during the duration of hydrothermal synthesis.

of gyrolite into wollastonite) increased up to 49.85 J/g by prolonging the hydrothermal treatment duration (120 h) (Fig. 3(b); Table 3). Also, the typical temperatures of this effect shift to higher temperatures: T_{onset} from 850°C to 857°C, T_{peak} from 862°C to 868°C, and T_{end} from 875°C to 878°C. Meanwhile, the weight loss of gyrolite varies from 0.30 to 0.20 wt%. It should be noted that the heat of

Table 2

Parameters of gyrolite endothermic effects at 80–200°C for varying durations of hydrothermal synthesis

Duration, h	T_{onset} , °C	T_{max} , °C	T_{end} , °C	Weight loss, wt%	Heat of reaction, J/g
32	108	138	176	5.54	48.68
48	108	144	176	5.08	55.75
72	110	143	175	4.67	70.87
120	111	143	175	3.90	71.09
168	115	145	177	3.56	69.34

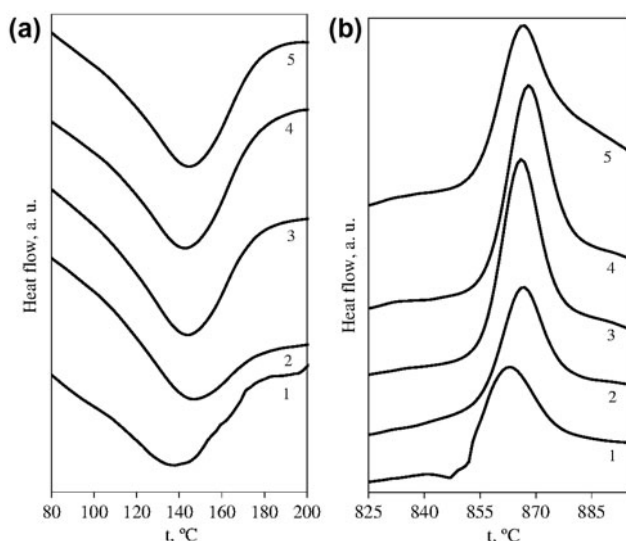


Fig. 3. DSC curves of gyrolite with varying duration of hydrothermal synthesis at 200°C, during h: 1–32, 2–48, 3–72, 4–120, 5–168.

exothermic effect was not changed by prolonging the duration of synthesis for one week (168 h).

It was observed that the duration of hydrothermal synthesis affected the form and size of the gyrolite crystals. The SEM analysis data showed that after 32 h and 48 h of isothermal curing the separated agglomerates (consisting of small crystal plates of size varying from 44 nm to 65 nm) were dominant in the synthesis

product (Fig. 4(a)). The crystal structure of gyrolite became more orderly structure after one week, and larger crystals ($>1 \mu\text{m}$) were observed (Fig. 4(b)). At the same time, the total amount of water in the gyrolite structure was decreased from 5.7 to 3.7 wt% (it is equal to 8.2–5.3 mol of H_2O in gyrolite composition) by prolonging the synthesis duration from 32 h to 168 h (Fig. 5). It should be emphasized that a linear regression model ($R^2 = 0.9764$) was fitted to the weight loss data.

Thus, gyrolite does not regroup into related compounds and remains stable when the hydrothermal synthesis duration varies from 32 to 168 h at 200°C, although its structure changes by prolonging the duration of synthesis. For this reason, the effect of gyrolite structure properties on zinc ion adsorption was investigated in the next stage of the experiment.

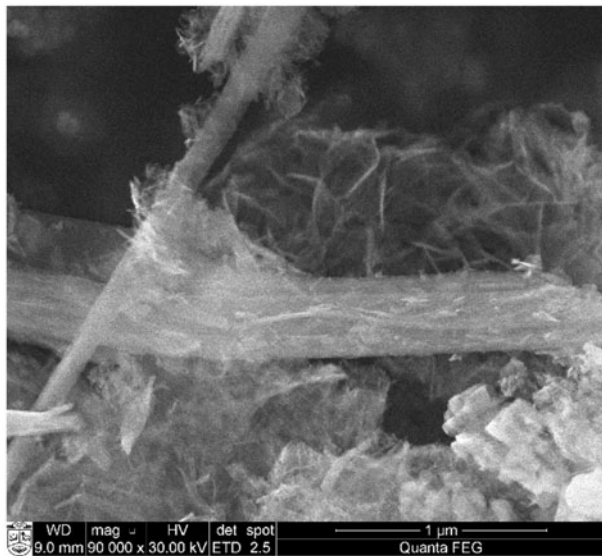
3.2. Gyrolite adsorption of Zn^{2+} ions in an alkaline solution

It was determined that after 30 s of adsorption about 88% (26.48 mg Zn^{2+} /g) of zinc ions were intercalated into the structure of gyrolite that was synthesized for 32 h (Fig. 6(a), curve 1). Meanwhile, the uptake of these ions into the orderly structure of gyrolite was much slower: 71% (21.36 mg Zn^{2+} /g) of zinc ions were intercalated into gyrolite synthesized for 72 h and only 56% (21.36 mg Zn^{2+} /g) into long-term synthesized (168 h) gyrolite. By the way, the adsorbent

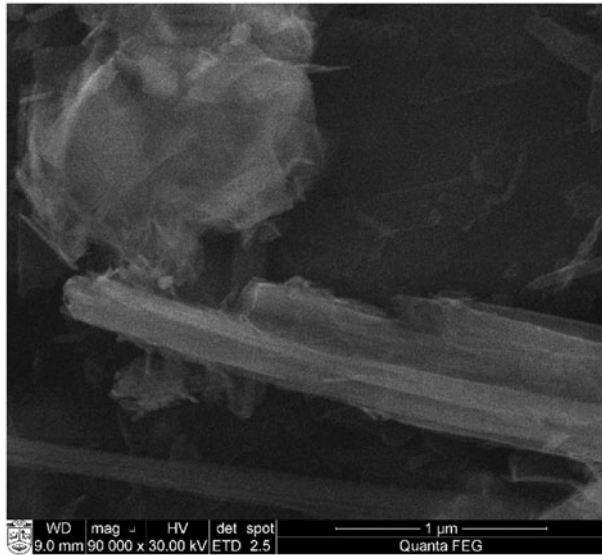
Table 3

Parameters of gyrolite exothermic effects at 830–890°C for varying durations of hydrothermal synthesis

Duration, h	T_{onset} , °C	T_{max} , °C	T_{end} , °C	Weight loss, wt%	Heat of reaction, J/g
32	850	862	875	0.30	25.23
48	855	867	877	0.20	31.49
72	856	866	875	0.20	48.27
120	857	868	878	0.20	49.85
168	855	866	876	0.20	49.90



(a)



(b)

Fig. 4. SEM micrographs of gyrolite with different durations of hydrothermal synthesis at 200°C, in h: (a) 32; (b) 168.

synthesis conditions have an effect on the total amount of adsorbed zinc ions in solution. For this reason, the maximum amount of adsorbed Zn²⁺ ions was two times higher using gyrolite synthesized for 32 h than by using long-term synthesized (168 h) gyrolite (Fig. 6(a), curve 5).

It should be noted that during the intrusion of zinc ions into the gyrolite structure, calcium ions are released from the crystal lattice of the adsorbent into solution. Most of the Ca²⁺ ions were released in the

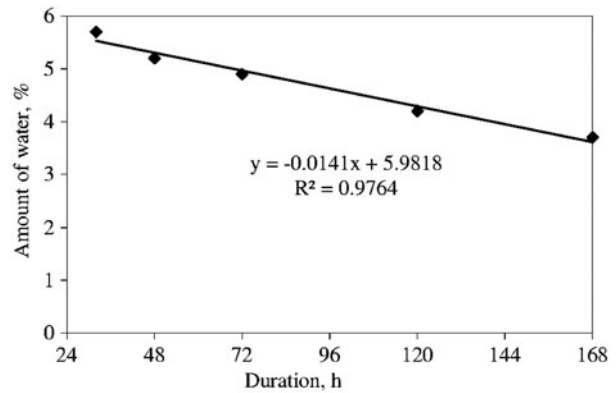


Fig. 5. Dependence of amount of water in gyrolite structure on the duration of hydrothermal synthesis.

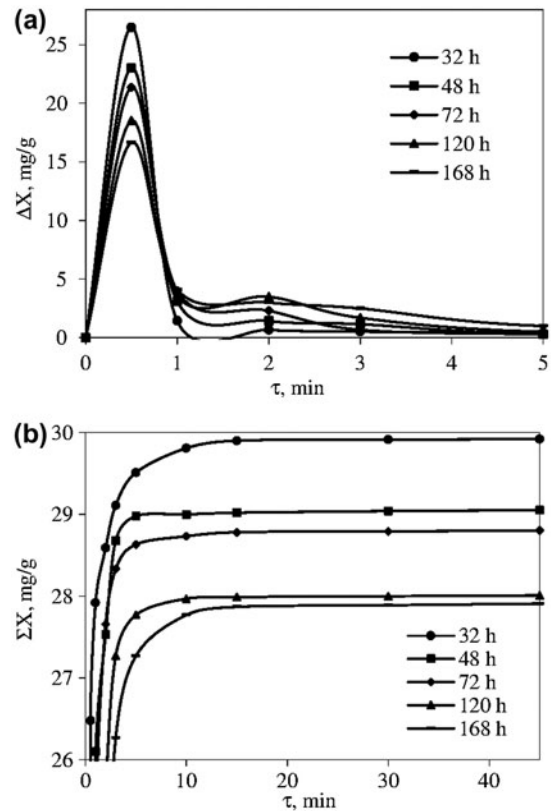


Fig. 6. Differential (a) and integral (b) kinetic curves during Zn²⁺ ion adsorption process at 200°C.

first minutes, and their amount slightly varies when the process of adsorption is prolonged (Fig. 7). It was determined that the largest amount of Ca²⁺ ions (15.09 mg Ca²⁺/g) was released into solution when using gyrolite synthesized for 32 h (Fig. 7(b), curve 1). As expected, the smallest amount of Ca²⁺ ions

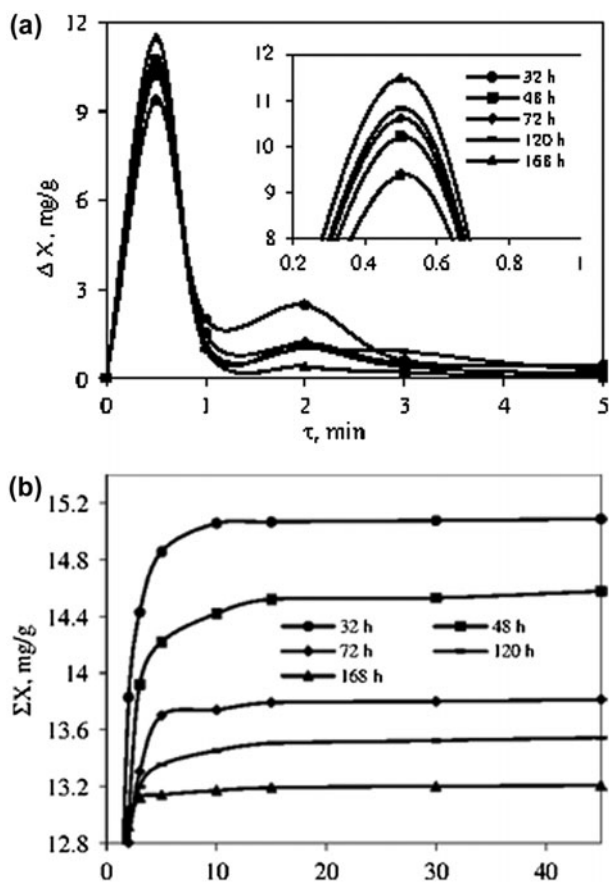


Fig. 7. Differential (a) and integral (b) kinetic curves during Ca^{2+} ion desorption process at 200°C .

($13.21 \text{ mg Ca}^{2+}/\text{g}$) was released when using gyrolite synthesized for one week (Fig. 7(a), curve 5).

It was determined that Zn^{2+} ions entered into the gyrolite structure by substitution ($\text{gyrolite-Ca}^0 + \text{Zn}^{2+} \leftrightarrow \text{gyrolite-Zn}^0 + \text{Ca}^{2+}$) and addition reactions. It was calculated that the zinc ions substituted for 5.42% of the Ca^{2+} ions in gyrolite synthesized for 32 h and for 3.87% when the duration of adsorbent synthesis was extended

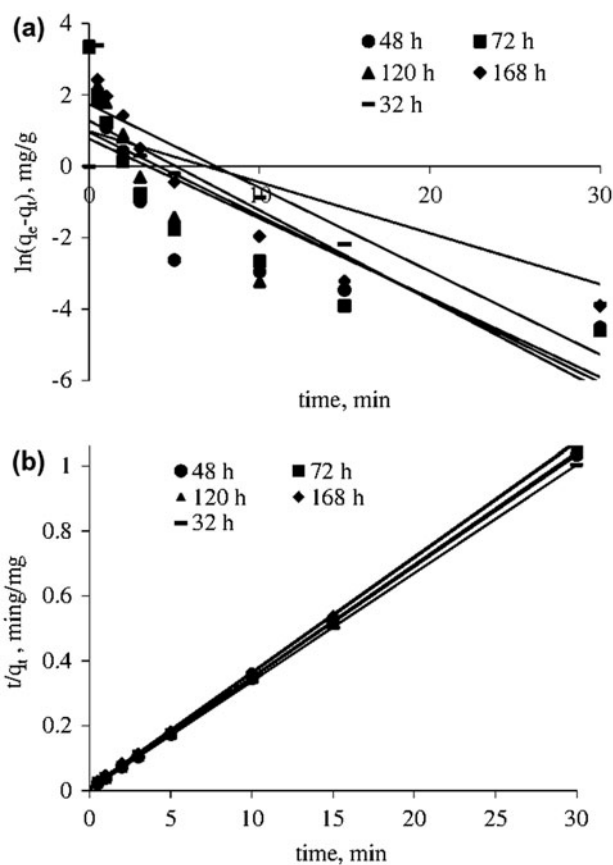


Fig. 8. Pseudo-first-order (a) and pseudo-second-order (b) kinetic plots for varying durations of synthesis.

(168 h), whereas the rest of these ions entered into the structure of gyrolite according to an addition interaction.

It should be noted that the adsorption reactions are not reversible processes. In order to confirm this fact, after the adsorption process (25°C , 45 min) the gyrolite with substituted zinc ions was dried and immersed in distilled water. It was proved that the mentioned ions did not appear in the solution after 45 min at 25°C .

Table 4

Kinetic parameters of the pseudo-first-order and pseudo-second-order-kinetic models for gyrolite

Duration of synthesis, h	$q_{e(\text{exp})}$	The pseudo first order			The pseudo second order		
		K_1	$q_{e(\text{cal})}$	R^2	K_2	$q_{e(\text{cal})}$	R^2
32	29.923	0.227	2.719	0.781	0.446	29.940	1.000
48	29.052	0.222	2.154	0.659	0.435	29.154	1.000
72	28.803	0.233	2.592	0.718	0.352	28.901	0.999
120	28.010	0.250	3.579	0.736	0.225	28.169	0.999
168	27.910	0.233	5.679	0.800	0.142	28.089	0.999

Note: $q_{e(\text{exp})}$ = amount of adsorbed ions, mg g^{-1} , calculated from experimental data; $q_{e(\text{cal})}$ = amount of adsorbed ions, mg g^{-1} , calculated by using Eqs. (3) and (4) of kinetic models.

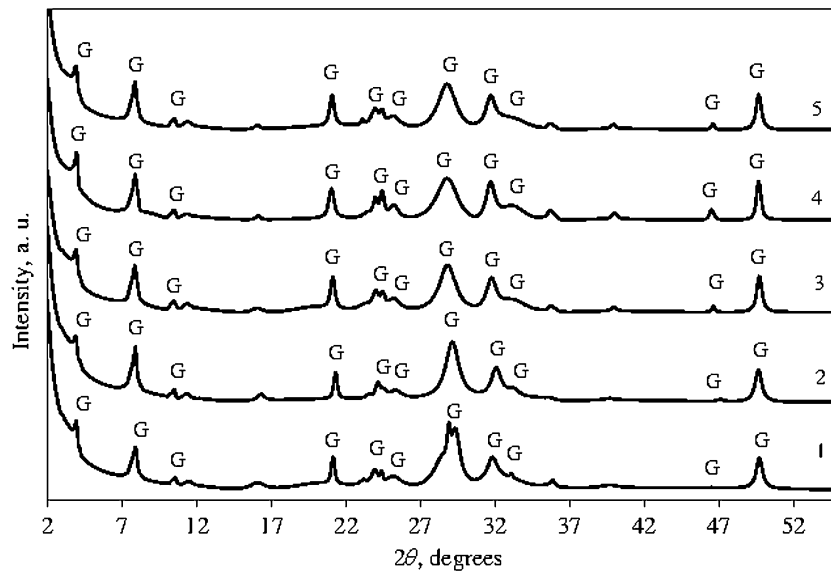


Fig. 9. X-ray diffraction patterns of gyrolite after adsorption process. Duration of hydrothermal synthesis at 200°C, in h: 1–32, 2–48, 3–72, 4–120, 5–168.

Thus, our research allows us to state that the adsorption reactions are specific to the chemisorption process. In order to determine adsorption kinetic parameters, kinetics models have been developed and fitted for the reactions of the Zn^{2+} ions by gyrolite.

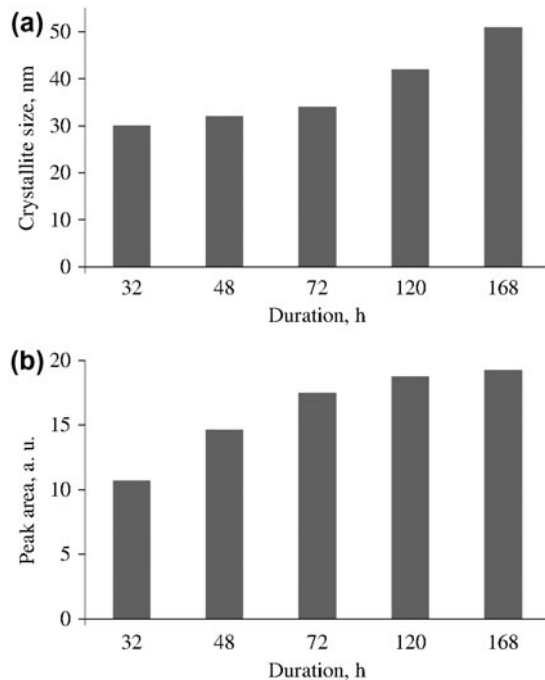


Fig. 10. Dependence of crystallite size (a) and diffraction peak area (001) (b) of gyrolite on the duration of hydrothermal synthesis after adsorption processes.

By using a pseudo-first-order kinetic rate equation in a linear form (Eq. 2), the amount of adsorbed ions ($q_{e(\text{exp})}$) and the first-order constants k_1 (min^{-1}) were determined experimentally from the slope and intercept plot of $\log(q_{e(\text{exp})} - q_t)$ vs. t (Fig. 8(a)). It was observed that the pseudo-first-order model did not fit well, because the calculated $q_{e(\text{cal})}$ values disagreed with the experimental $q_{e(\text{exp})}$ values, and the values of the correlation coefficient (R^2) were very low (from 0.781 to 0.8) (Table 4).

Using the pseudo-second-order kinetics equation (Eq. 4), the amount of adsorbed ions ($q_{e(\text{exp})}$) and the second-order constants k_2 ($\text{g mg}^{-1} \text{min}^{-1}$) were determined experimentally from the slope and intercept of plot t/q_t vs. t (Fig. 8(b)). The values of the calculated $q_{e(\text{cal})}$ and experimental $q_{e(\text{exp})}$ are represented in Table 4.

An agreement between $q_{e(\text{exp})}$ experimental and $q_{e(\text{cal})}$ calculated values for the pseudo-second-order model was observed. Also, the adsorption rate constant (k_2) decreased from 0.446 to 0.142 by prolonging the duration of synthesis from 32 h to 168 h. The calculated values of the adsorption rate constant confirmed the experimental data: the synthesis conditions of gyrolite affect its adsorption capacity for zinc ions, because the ion intercalation proceeds with more difficulty when using gyrolite with a more orderly structure.

In order to identify the stability of gyrolite, the products of adsorption were characterized by XRD analysis (Fig. 9).

It was determined that the structure of gyrolite remained stable, because the most characteristic peak (d -spacing = 2.273 nm) did not change over the varying durations of the adsorption reactions (Fig. 9(a), curve 2).

It was determined that, after the adsorption process, the crystallite size and diffraction peak area (001) of gyrolite decreased about 51 nm and 19 a. u., respectively, under all synthesis conditions (Fig. 10(a) and (b)).

This change is attributed to the degree of release of Ca^{2+} ions from the gyrolite solid into solution, and of Zn^{2+} ion intercalation into the orderly structure of the gyrolite. These data confirm previous results that Zn^{2+} ions entered into the gyrolite structure by substitution and addition reactions.

4. Conclusions

- (1) It was found that gyrolite did not regroup into related compounds and remained stable when the hydrothermal synthesis duration varied from 32 to 168 h at 200°C. However, its structure changed: the crystallite size almost doubled (up to 95 nm). Meanwhile, the specific heat of endothermal effect at 80°C–200°C changed from 48.68 to 71.09 J/g, and the total water content in its structure decreased from 5.7 to 3.7 wt%.
- (2) It was determined that the synthesis conditions of gyrolite affected its adsorption capacity for zinc ions. By prolonging the duration of synthesis from 32 to 168 h, the adsorption capacity of gyrolite decreased from 99% (29.92 mg Zn^{2+} /g) to 93% (27.91 mg Zn^{2+} /g), respectively. It was found that Zn^{2+} ions were intercalated into the gyrolite structure by substitution (gyrolite- $\text{Ca}^0 + \text{Zn}^{2+} \leftrightarrow$ gyrolite- $\text{Zn}^0 + \text{Ca}^{2+}$) and addition reactions. It was calculated that Zn^{2+} ions substituted for 5.42% of Ca^{2+} ions in gyrolite synthesized for 32 h and for 3.87% when the duration of adsorbent synthesis was extended (168 h), whereas the rest of the Zn^{2+} ions entered the structure of gyrolite by an addition interaction.
- (3) It was found that the adsorption reactions are not reversible processes and follow a pseudo-second-order model. In addition, the properties of the gyrolite structure have an effect on the adsorption rate constant (k_2) that decreased from 0.446 to 0.142, when prolonging the duration of the synthesis from 32 to 168 h.

Acknowledgement

The present work was funded by a grant (No. MIP-025/2014) from the Research Council of Lithuania.

References

- [1] D. Han, X. Zhang, S. Tomar Vijay Vikram, Q. Li, D. Wen, W. Liang, Effects of heavy metal pollution of highway origin on soil nematode guilds in North Shenyang, China, *J. Environ. Sci.* 21 (2009) 193–198.
- [2] T. Hosono, C. Su, F. Siringan, A. Amano, S. Onodera, Effects of environmental regulations on heavy metal pollution decline in core sediments from Manila Bay, *Mar. Pollut. Bull.* 60 (2010) 780–785.
- [3] S. Audry, J. Schäfer, G. Blanc, J.M. Jouanneau, Fifty-year sedimentary record of heavy metal pollution (Cd, Zn, Cu, Pb) in the Lot River reservoirs (France), *Environ. Pollut.* 132 (2004) 413–426.
- [4] J.-H. Ma, C.-J. Chu, J. Li, B. Song, Heavy metal pollution in soils on railroad side of Zhengzhou-Putian section of Longxi-Haizhou railroad, China, *Pedosphere* 19 (2009) 121–128.
- [5] T.R. Chen, K.F. Yu, S. Li, G.J. Price, Q. Shi, G.J. Wei, Heavy metal pollution recorded in Porites corals from Daya Bay, northern South China Sea, *Mar. Environ. Res.* 70 (2010) 318–326.
- [6] K.K. Sivakumar, M.S. Dheenadayalan, C. Balamurugan, R. Kalaivani, D. Ramakrishnan, L. Hebsi bai Leena, Environmental water pollution: A review of physico-chemical and heavy metal quality of water and soil, *J. Chem. Biol. Phys. Sci.* 2 (2012) 1079–1090.
- [7] W.D. Macdonald, O.E. Christopher, Pollution studies on Nigerian rivers: Heavy metals in surface water of Warri river, Delta State, *J. Biodivers Environ. Sci.* 1 (2011) 7–12.
- [8] O. Oladele, D.P. Adegbenro, G.M. Adewole, The impact of industries on surface water quality of River Ona and River Alaro in Oluyole Industrial Estate, Ibadan, Nigeria, *Afr. J. Biotechnol.* 10 (2012) 696–702.
- [9] Z. Li, Z. Ma, T.J. van der Kuip, Z. Yuan, L. Huang, A review of soil heavy metal pollution from mines in China: Pollution and health risk assessment, *Sci. Total Environ.* 468–469 (2014) 843–853.
- [10] S.K. Agarwal, Heavy Metal Pollution, APH Publishing Corporation, New Delhi, 2009.
- [11] E. Katsou, S. Malamis, M. Tzanoudaki, K.J. Haralambous, M. Loizidou, Regeneration of natural zeolite polluted by lead and zinc in wastewater treatment systems, *J. Hazard. Mater.* 189 (2011) 773–786.
- [12] J. Van den Berge, K. Naudts, I.A. Janssens, R. Ceulemans, I. Nijs, Does the stress tolerance of mixed grassland communities change in a future climate? A test with heavy metal stress (zinc pollution), *Environ. Pollut.* 159 (2011) 3294–3301.
- [13] S. Megateli, S. Semsari, M. Couderchet, Toxicity and removal of heavy metals (cadmium, copper, and zinc) by Lemna gibba, *Ecotoxicol. Environ. Saf.* 72 (2009) 1774–1780.
- [14] H. Cesur, N. Balkaya, Zinc removal from aqueous solution using an industrial by-product phosphogypsum, *Chem. Eng. J.* 131 (2007) 203–208.

- [15] L. Peng, D. Sun, M. Su, J. Han, C. Dong, Rapid analysis on the heavy metal content of spent zinc–manganese batteries by laser-induced breakdown spectroscopy, *Opt. Laser Technol.* 44 (2012) 2469–2475.
- [16] S.F. Montanher, E.A. Oliveira, M.C. Rollemberg, Removal of metal ions from aqueous solutions by sorption onto rice bran, *J. Hazard. Mater.* 117 (2005) 207–211.
- [17] V. Arambula-Villazana, M.T. Olguin, Sorption of cadmium from aqueous solutions at different temperatures by mexican HEU-type zeolite rich tuff, *J. Inclusion Phenom. Macrocyclic Chem.* 55 (2006) 237–245.
- [18] M.A. Barakat, New trends in removing heavy metals from industrial wastewater, *Arab. J. Chem.* 4 (2010) 361–377.
- [19] M. Malakootian, J. Nouri, H. Hossaini, Removal of heavy metals from paint industry's wastewater using Leca as an available adsorbent, *Int. J. Environ. Sci. Technol.* 6 (2009) 183–190.
- [20] S. Sen Gupta, K.G. Bhattacharyya, Immobilization of Pb(II), Cd(II), and Ni(II) ions on kaolinite and montmorillonite surfaces from aqueous medium, *J. Environ. Manage.* 87 (2008) 46–58.
- [21] N.J. Coleman, C.J. Trice, J.W. Nicholson, 11 Å tobermorite from cement bypass dust and waste container glass: A feasibility study, *Int. J. Miner. Process.* 93 (2009) 73–78.
- [22] S.A. El-Korashy, Hydrothermal synthesis and transition metal cations exchange characterization of titanium and [titanium+alkali metals] substituted-11Å tobermorites, *J. Korean Chem. Soc.* 48 (2004) 129–136.
- [23] S.A. El-Korashy, Synthetic crystalline calcium silicate hydrate (I): Cation exchange and caesium selectivity, *Chem. Mon.* 133 (2002) 333–343.
- [24] N.Y. Mostafa, E.A. Kishar, S.A. Abo-El-Enein, FTIR study and cation exchange capacity of Fe³⁺- and Mg²⁺-substituted calcium silicate hydrates, *J. Alloys Compd.* 473 (2009) 538–542.
- [25] S. Merlino, Gyrolite: Its crystal structure and crystal chemistry, *Mineral. Mag.* 52 (1988) 377–387.
- [26] K. Baltakys, R. Siauciunas, The influence of stirring and γ -Al₂O₃ or Na₂O additives on the gyrolite formation in the CaO–quartz–H₂O system, *Ceram. Silik.* 51 (2007) 106–111.
- [27] A. Eisinas, K. Baltakys, R. Siauciunas, The effect of gyrolite additive on the hydration properties of Portland cement, *Cem. Concr. Res.* 42 (2012) 27–38.
- [28] K. Baltakys, A. Eisinas, T. Dizhbite, L. Jasina, R. Siauciunas, S. Kitrys, The influence of hydrothermal synthesis conditions on gyrolite texture and specific surface area, *Mater. Struct.* 44 (2011) 1687–1701.
- [29] S. Shaw, C.M.B. Henderson, S.M. Clark, *In-situ* synchrotron study of the kinetics, thermodynamics, and reaction mechanisms of the hydrothermal crystallization of gyrolite, *Am. Mineral.* 87 (2002) 533–541.
- [30] M. Baltakys, R. Siauciunas, R. Jauberthie, K. Baltakys, The influence of Zn containing components on the synthesis of Z-phase, *Sci. Sintering.* 45 (2013) 49–60.
- [31] A. Bankauskaite, K. Baltakys, The sorption of copper ions by gyrolite in alkaline solution, *Mater. Sci. Poland.* 27 (2009) 899–908.
- [32] V. Kasperaviciute, K. Baltakys, R. Siauciunas, The sorption properties of gyrolite for copper ions, *Ceram. Silik.* 52 (2008) 95–101.
- [33] S. Malamis, E.A. Katsou, A review on zinc and nickel adsorption on natural and modified zeolite, bentonite and vermiculite: Examination of process parameters, kinetics and isotherms, *J. Hazard. Mater.* 252–253 (2013) 428–461.
- [34] E.S. Abechi, C.E. Gimba, A. Uzairu, J.A. Kagbu, Kinetics of adsorption of methylene blue onto activated carbon prepared from palm kernel shell, *Arch. Appl. Sci. Res.* 3 (2011) 154–164.
- [35] B.H. Hameed, D.K. Mahmoud, A.L. Ahmad, Equilibrium modeling and kinetic studies on the adsorption of basic dye by a low-cost adsorbent: Coconut (*Cocos nucifera*) bunch waste, *J. Hazard. Mater.* 158 (2008) 65–72.
- [36] R. Siauciunas, K. Baltakys, Formation of gyrolite during hydrothermal synthesis in the mixtures of CaO and amorphous SiO₂ or quartz, *Cem. Concr. Res.* 34 (2004) 2029–2036.
- [37] R. Vinodkumar, I. Navas, K. Porsezian, V. Ganesan, N.V. Unnikrishnan, V.P. Mahadevan Pillai, Structural, spectroscopic and electrical studies of nanostructured porous ZnO thin films prepared by pulsed laser deposition, *Spectrochim. Acta Part A*, 118 (2014) 724–732.